

Article

Efficient Method for the Concentration Determination of Fmoc Groups Incorporated in the Core-Shell Materials by Fmoc–Glycine

Elżbieta Szczepańska¹, Beata Grobelna¹, Jacek Ryl² , Amanda Kulpa¹, Tadeusz Ossowski¹ and Paweł Niedziałkowski^{1,*} 

¹ Department of Analytical Chemistry, Faculty of Chemistry, University of Gdansk, Wita Stwosza 63, 80-308 Gdansk, Poland; elzbieta.szczepanska@phdstud.ug.edu.pl (E.S.); beata.grobelna@ug.edu.pl (B.G.); amanda.kulpa@phdstud.ug.edu.pl (A.K.); tadeusz.ossowski@ug.edu.pl (T.O.)

² Corrosion and Materials Engineering, Department of Electrochemistry, Faculty of Chemistry, Gdansk University of Technology, Narutowicza 11/12, 80-233 Gdansk, Poland; jacek.ryl@pg.edu.pl

* Correspondence: pawel.niedzialkowski@ug.edu.pl; Tel.: +48-58-523-5100

Academic Editors: Amay J. Bandodkar and Byoung-Suhk Kim

Received: 23 July 2020; Accepted: 31 August 2020; Published: 1 September 2020



Abstract: In this paper, we described the synthesis procedure of TiO₂@SiO₂ core-shell modified with 3-(aminopropyl)trimethoxysilane (APTMS). The chemical attachment of Fmoc–glycine (Fmoc–Gly–OH) at the surface of the core-shell structure was performed to determine the amount of active amino groups on the basis of the amount of Fmoc group calculation. We characterized nanostructures using various methods: transmission electron microscope (TEM), scanning electron microscopy (SEM), Fourier-transform infrared spectroscopy (FTIR), thermogravimetric analysis (TGA) and X-ray photoelectron spectroscopy (XPS) to confirm the modification effectiveness. The ultraviolet-visible spectroscopy (UV-vis) measurement was adopted for the quantitative determination of amino groups present on the TiO₂@SiO₂ core-shell surface by determination of Fmoc substitution. The nanomaterials were functionalized by Fmoc–Gly–OH and then the fluorenylmethoxycarbonyl (Fmoc) group was cleaved using 20% (*v/v*) solution of piperidine in DMF. This reaction led to the formation of a dibenzofulvene–piperidine adduct enabling the estimation of free Fmoc groups by measurement the maximum absorption at 289 and 301 nm using UV-vis spectroscopy. The calculations of Fmoc loading on core-shell materials was performed using different molar absorption coefficient: 5800 and 6089 dm³ × mol^{−1} × cm^{−1} for λ = 289 nm and both 7800 and 8021 dm³ × mol^{−1} × cm^{−1} for λ = 301 nm. The obtained results indicate that amount of Fmoc groups present on TiO₂@SiO₂–(CH₂)₃–NH₂ was calculated at 6 to 9 μmol/g. Furthermore, all measurements were compared with Fmoc–Gly–OH used as the model sample.

Keywords: loading of amino groups; Fmoc–Gly–OH; TiO₂@SiO₂ core-shell; dibenzofulvene–piperidine adduct; nanoparticles

1. Introduction

Titanium dioxide (TiO₂) possesses many advantages, is nontoxic, highly efficient, photocatalytically stable and cost-effective [1,2]. Therefore, this compound has been extensively used in many fields. Recently, TiO₂ has found several applications, including the development of new fluorescent materials [3,4], UV filters for cosmetics and paint pigments, [5] or photocatalysts used for water and air purification [6].

Nowadays, various metal nanoparticles such as silver, gold or titanium are widely used not only in industry, but also in nanotechnology and other various fields of research [7,8]. The titanium

dioxide nanoparticles (TiO₂ NPs) are utilized in many fields of industry [9]. Nevertheless, one of the biggest drawbacks of TiO₂ NPs is the tendency to agglomerate. This limitation has been solved by the deposition of TiO₂ NPs on surfaces of other materials such as silica (SiO₂) resulting in the formation of TiO₂@SiO₂ core-shell particles. The SiO₂ coating of NPs provides the colloidal stability, but the presence of silanol groups on the NPs surface contribute to the possible additional modification by various functional groups such as: alkyl [10], hydroxyl [11], thiol (-SH) [12,13], carboxyl (-COOH) [14], amine (-NH₂) [15], EDTA derivatives [16] or other nanoparticles and ions [17,18].

3-(Aminopropyl)trimethoxysilane (APTES) is one of the most popular agents used for modifications of various nanoparticles such as TiO₂ NPs [19], Fe₃O₄ [20], glass [21] or solid electrodes [22]. The presence of amino silane after reaction with hydroxyl-terminated surface makes it possible to obtain a new material with terminal amino groups. Consequently, these amino groups enable the immobilization of new biomolecules, such as proteins [23], enzymes [24], antibodies [25,26] or DNA samples [27].

The mechanism of NPs modification by alkoxysilanes consists of two steps. The first process is associated with the hydrolysis of silane groups of used modification agent which leads to the formation of alcohol and active alkoxysilane derivative. The second step leads to the condensation of organosilanols with hydroxyl groups present on the modified NPs surface. In this step, the condensation process also occurs [28]. The mechanism of action for APTES is based on the reaction with the hydroxyl group of the oxidized surface by SN₂ exchange and loss of ethanol. The same reaction is observed in the case of APTMS usage, but during the surface covering the methanol is formed as a byproduct. The detailed studies of APTES hydrolysis and then condensation, including various details such as time reaction, concentration, temperature or pH is described elsewhere [25,29–31].

In the synthesis of modified nanoparticles—as well as in immobilization of biomolecules onto the surface—an important parameter characterizing the modified material is the estimation of the number of functional groups deposited on the surface to assess further modifications or material analyses. Determination of the amino group concentration is the most important parameter after modification by amino silanes. Estimation of amino groups can be obtained by various analytical methods, including acid–base back titration or reaction [32], conductometric titrations [33], NMR [34] or ζ-potential and direct measurements [35], thermogravimetric analysis [36] or X-ray photoelectron spectroscopy (XPS) analysis [37].

Additionally, amino functional groups can be estimated using various analytical methods after chemical reaction described above. The absorbance measurements after reaction with fluorescent rhodamine B isothiocyanate [32], the ninhydrin assay, as well as 4-nitrobenzaldehyde assay and NMR measurements are exceptionally useful for the determination of the amino functional groups [38]. Nevertheless, all of these methods show various sensitivities and advantages, but the main limitation of the methods listed above is the small amount of NPs for analyses.

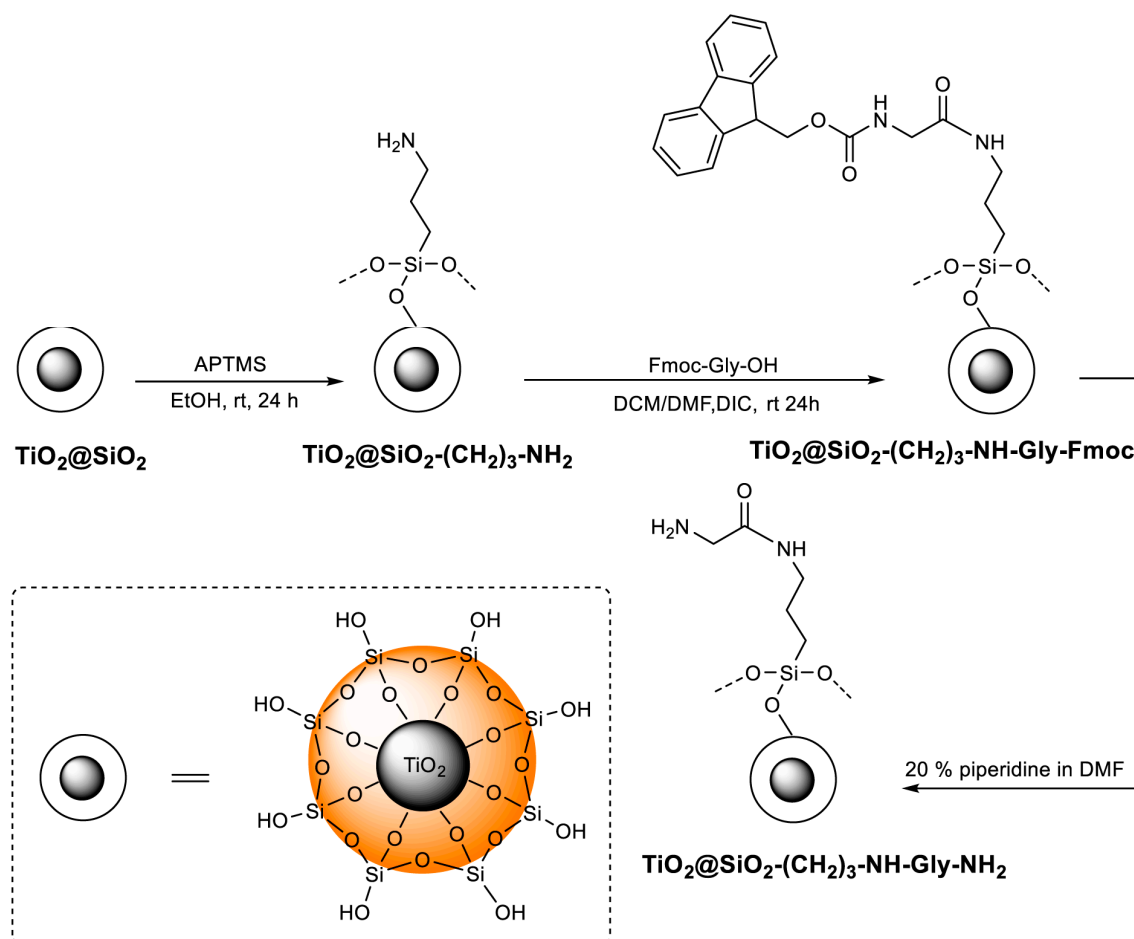
In this work, we obtained TiO₂@SiO₂ core-shell by Stöber method. The main advantage of the Stöber method based on sol–gel chemistry is simplicity, wide availability of reagents and possibility of obtaining three-dimensional materials such as core shell nanoparticles in a one-pot synthesis. This method allow to obtain nanostructures with nano to micrometers size [39].

Subsequently, obtained TiO₂@SiO₂ core-shell was modified using (3-aminopropyl)trimethoxysilane (APTMS) to determine Fmoc groups concentration, what enabled the estimation of the amino group presence on the surface. Nowadays, the estimation of amino group presence on the surface of amino-modified nanomaterials is very problematic and requires much effort and instruments. Therefore, the nanoparticles were functionalized by Fmoc–Gly–OH and then Fmoc group was cleaved using 20% (v/v) piperidine solution in DMF. This reaction led to the formation of dibenzofulvene–piperidine adduct, used for the estimation of free amino groups by the measurement of the maximum absorption at 289 and 301 nm. The obtained results indicate that amount of Fmoc groups present on TiO₂@SiO₂–(CH₂)₃–NH₂ was calculated at 6 to 9 μmol/g. All measurements were also compared with the solution of Fmoc–Gly–OH used as the model sample.

2. Results and Discussion

2.1. Synthesis

The synthesis and modification steps of TiO₂ NPs are presented on Scheme 1. The TiO₂ NPs were obtained in the reaction of titanium (IV) isopropoxide (TTIP) used as a titanium source and SDS as a surfactant by the microemulsion method previously described in Yuenyongsuwan procedure [40].



Scheme 1. Synthesis of TiO₂@SiO₂ with (3-aminopropyl)trimethoxysilane (APTMS), Fmoc-Gly-OH and cleavage by piperidine in 20% (*v/v*) solution in DMF.

TiO₂ NPs obtained using this method were used for further modifications. The TiO₂@SiO₂ core-shell structures were synthesized using Stöber method [41] with tetraethyl orthosilicate (TEOS) in the solution of pH = 9 adjusted by ammonia hydroxide.

In described Stöber method the core shell nanostructures are formed by hydrolysis and condensation of TEOS in ethanol and water catalyzed by ammonia hydroxide at room temperature [39,42].

The TiO₂@SiO₂ core-shell structures in this work were obtained by the adoption of the method described for the preparation of Ag@SiO₂ core-shell nanoparticles [43].

In the next step, the obtained core-shell TiO₂@SiO₂ nanostructures were modified by an aminosilanization process using the post-grafting method with 3-(aminopropyl)trimethoxysilane (APTMS) as the reagent [44]. After the completion of the reaction, the presence of amino groups was confirmed using chloranil test performed on TiO₂@SiO₂-(CH₂)₃-NH₂ with microscopic magnification [45]. Figure 1 shows the comparison of chloranil test performed for TiO₂@SiO₂ and TiO₂@SiO₂-(CH₂)₃-NH₂ and its microscopic magnification. The chloranil test used in our experiments was consist of equally volumetric amounts of 2% solutions acetaldehyde in DMF and 2% solution

of p-chloranil dissolved in DMF. After 15 min the change of colors from white to greenish blue was observed for $\text{TiO}_2@SiO_2-(CH_2)_3-NH_2$ NPs indicating the presence of amino groups. On the other hand, the change of color for core-shell $\text{TiO}_2@SiO_2$ nanostructure were not observed due to the fact of absence of amino group.

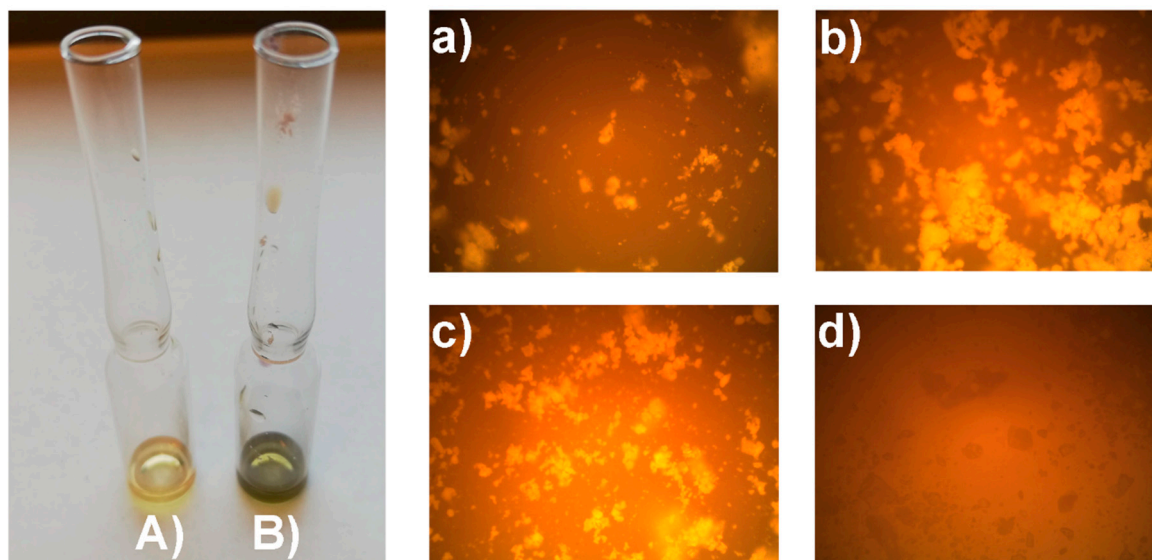


Figure 1. Chloranil test performed for (A) $\text{TiO}_2@SiO_2$ and (B) $\text{TiO}_2@SiO_2-(CH_2)_3-NH_2$. The microscopic magnification for core-shell $\text{TiO}_2@SiO_2$ nanostructures (a) before and (b) after chloranil test and for $\text{TiO}_2@SiO_2-(CH_2)_3-NH_2$ NPs (c) before and (d) after chloranil test.

Subsequently, the modified $\text{TiO}_2@SiO_2-(CH_2)_3-NH_2$ NPs were used for coupling with Fmoc-glycine (Fmoc-Gly-OH). This reaction was performed in a solution consisting of methylene chloride: DMF, 1:1, (*v/v*) in the presence of 4-dimethylaminopyridine (DMAP) and diisopropylcarbodiimide (DIC) obtaining $\text{TiO}_2@SiO_2-(CH_2)_3-NH-Gly-Fmoc$. This procedure is used in peptide chemistry for the attachment of amino acids for resins calculations [46]. The Fmoc deprotection was performed using 20% (*v/v*) piperidine in DMF commonly used in the solid-phase peptide synthesis [47].

2.2. Analysis of Obtained Nanoparticles

TiO_2 nanostructures as well as other studied nanoparticles were characterized using scanning electron microscopy (SEM). SEM images presented in Figure 2 show the presence of nanoparticles in the highly aggregated state.

No significant differences between the nanoparticles are not observed after each step of modifications. Therefore, in order to receive more precise visualization of studied nanoparticles surface the TEM images were obtained (Figure 3). SEM analysis of all nanoparticles were performed for powders, while TEM images were obtained for the nanoparticle suspensions which influence on the behavior of studied nanostructures.

The TEM images of three kinds of nanostructures— TiO_2 , $\text{TiO}_2@SiO_2$, and $\text{TiO}_2@SiO_2-(CH_2)_3-NH_2$ —are presented in Figure 3. The structure of $\text{TiO}_2@SiO_2-(CH_2)_3-NH-Gly-Fmoc$ is strikingly similar to $\text{TiO}_2@SiO_2-(CH_2)_3-NH_2$, thus these images are not presented.

All nanoparticles have a spherical shape, but they significantly differ in the aggregation levels. We can observe that aggregation into larger clusters decreased with the modification degree. The highest aggregation is observed in the decreasing order for $\text{TiO}_2@SiO_2-(CH_2)_3-NH_2$, $\text{TiO}_2@SiO_2$ and TiO_2 . The covering of TiO_2 nanoparticles by silica core-shell structures and further modification by APTMS prevent the aggregation process [48,49].

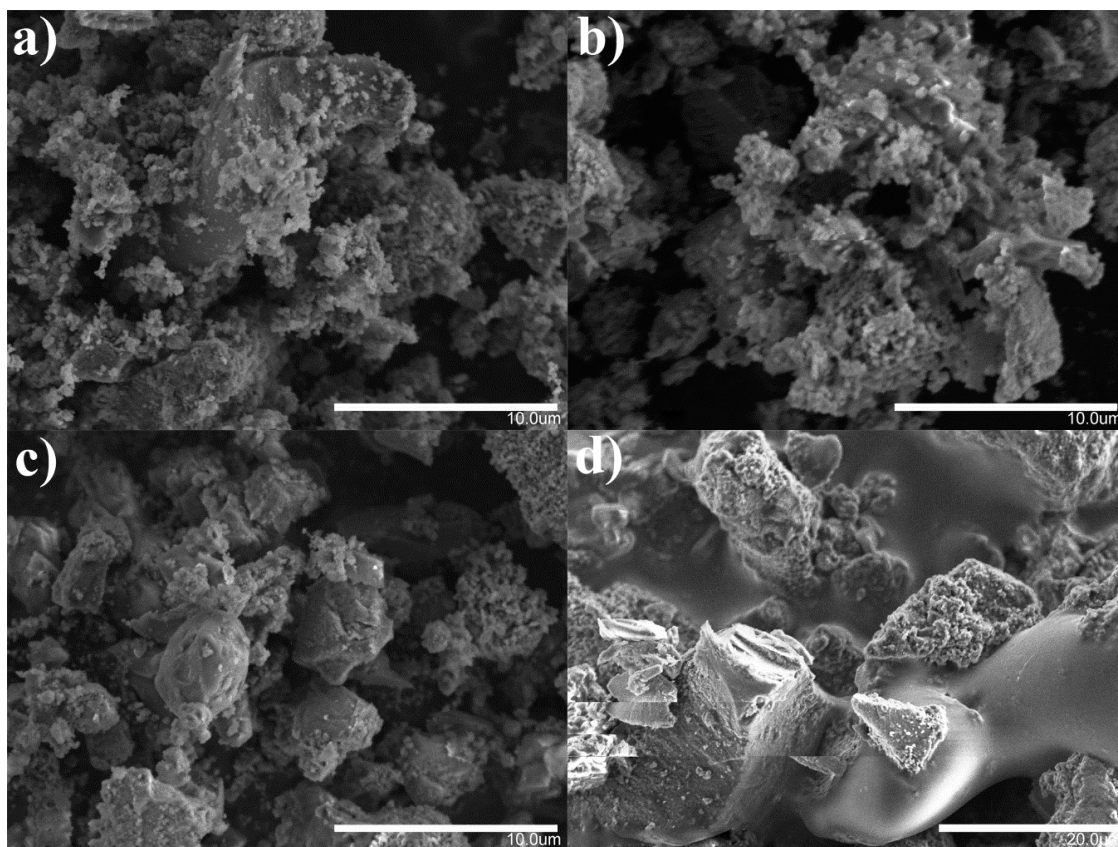


Figure 2. Scanning electron microscopy (SEM) images of (a) TiO_2 , (b) $\text{TiO}_2@SiO_2$, (c) $\text{TiO}_2@SiO_2-(CH_2)_3-NH_2$ and (d) $\text{TiO}_2@SiO_2-(CH_2)_3-NH-Gly-Fmoc$.

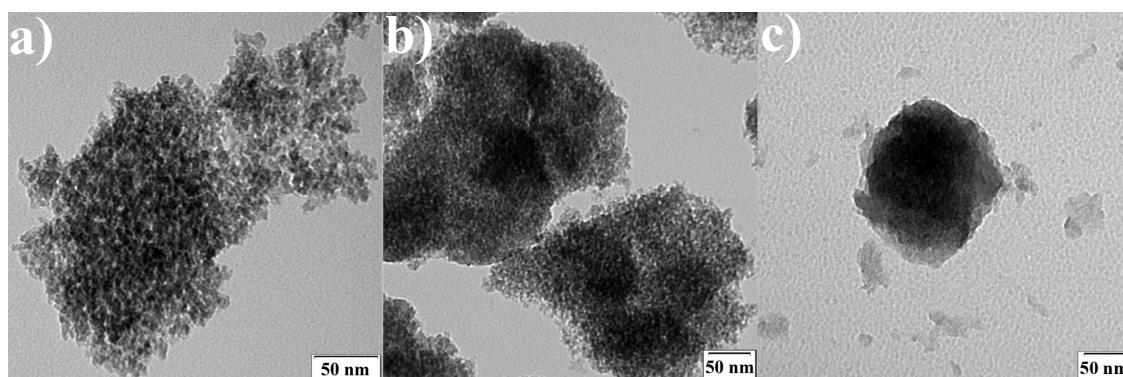


Figure 3. Transmission electron microscopy (TEM) images of (a) TiO_2 , (b) $\text{TiO}_2@SiO_2$ and (c) $\text{TiO}_2@SiO_2-(CH_2)_3-NH_2$.

The average size of nanoparticles is about 10 nm for TiO_2 , $\text{TiO}_2@SiO_2$ and 100 nm for $\text{TiO}_2@SiO_2-(CH_2)_3-NH_2$.

Figure 4 shows a sequence of FTIR spectra for TiO_2 , $\text{TiO}_2@SiO_2$, $\text{TiO}_2@SiO_2-(CH_2)_3-NH_2$ and $\text{TiO}_2@SiO_2-(CH_2)_3-NH-Gly-Fmoc$ the characteristic bands of TiO_2 were observed Figure 4a. The broadband region located at the 3380 cm^{-1} is related to the stretching vibration of the hydroxyl group (-OH). The band at the 1633 cm^{-1} is assigned to bending modes of Ti-OH water. Additionally, the last band located at 620 cm^{-1} range represents the stretching vibrations of Ti-O-Ti binding [50,51]. However, the FTIR spectrum of $\text{TiO}_2@SiO_2$ —presented in Figure 4a—shows more absorption bands in comparison with the absorption bands observed for the titanium dioxide. The characteristic bands at 3450 cm^{-1} and 1600 cm^{-1} in the spectra are attributed to the stretching vibration and bending vibration

of hydroxyl groups. The band at 1400 cm^{-1} was assigned as the Ti–O–Ti vibration [52]. The peaks at 1080 cm^{-1} , 950 cm^{-1} and 470 cm^{-1} correspond to the stretching vibrations for Si–O–Si, Ti–O–Si and Ti–O, respectively [53]. Figure 4b presents $\text{TiO}_2@\text{SiO}_2-(\text{CH}_2)_3-\text{NH}_2$ particles. The peak at 3400 cm^{-1} is associated with $-\text{NH}_2$ stretching vibrations and the peaks at 2930 cm^{-1} are assigned to the stretching vibrations of $-\text{CH}_2$ groups. The absorption band at 1600 cm^{-1} is associated with the presence of $-\text{NH}_2$ deformation mode [54]. Furthermore, the absorption peaks at 1130 and 1030 cm^{-1} belong to Si–O–Si, peak at 690 cm^{-1} was assigned to the stretching vibration of the Ti–O–Ti bond, the Ti–O group is observed at 460 cm^{-1} . For $\text{TiO}_2@\text{SiO}_2-(\text{CH}_2)_3-\text{NH}-\text{Gly}-\text{Fmoc}$ (Figure 4b) similar bands are observed as in the case of $\text{TiO}_2@\text{SiO}_2-(\text{CH}_2)_3-\text{NH}_2$. One of the most characteristic peaks is observed at 1660 cm^{-1} which presents stretching groups combined with carbonyl groups ($-\text{C}=\text{O}$) [55]. This analysis confirmed the modification of TiO_2 with silica, amino groups and Fmoc–Gly–OH.

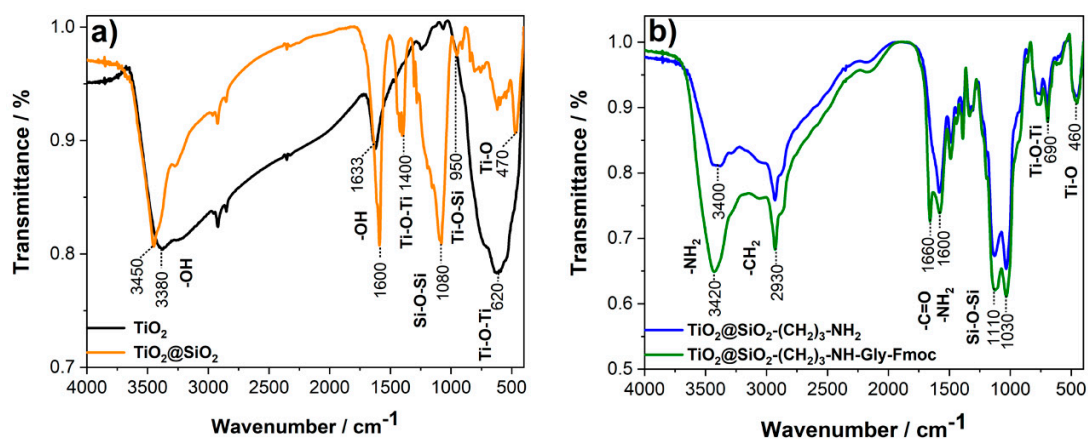


Figure 4. Fourier-transform infrared spectra of (a) TiO_2 , $\text{TiO}_2@\text{SiO}_2$ and (b) $\text{TiO}_2@\text{SiO}_2-(\text{CH}_2)_3-\text{NH}_2$, $\text{TiO}_2@\text{SiO}_2-(\text{CH}_2)_3-\text{NH}-\text{Gly}-\text{Fmoc}$.

Thermogravimetric analysis (TGA) and derivative thermogravimetric analysis (DTG) for TiO_2 , $\text{TiO}_2@\text{SiO}_2$ and $\text{TiO}_2@\text{SiO}_2-(\text{CH}_2)_3-\text{NH}_2$ is presented at Figure 5. For TiO_2 NPs, the 7.92% weight loss is observed between 65 and $200\text{ }^\circ\text{C}$, this process is probably associated with physical desorption of water on the surface [49]. Next visible changes are observed within the range 300 to $410\text{ }^\circ\text{C}$ with the weight loss of 5.28% attributed to the reduction of hydroxyl groups.

For $\text{TiO}_2@\text{SiO}_2$ core-shell, 6.65% weight loss in the 350 to $500\text{ }^\circ\text{C}$ range indicates the disintegration of hydroxyl groups in silanol moieties [56]. The range of 500 to $700\text{ }^\circ\text{C}$ is characterized with the weight loss of 2.74% due to the degradation of $-\text{CH}_2\text{CH}_3$ alkyl group in TEOS [49].

In the case of $\text{TiO}_2@\text{SiO}_2-(\text{CH}_2)_3-\text{NH}_2$ structure, the largest decrease in mass of 14.01% within 400 to $600\text{ }^\circ\text{C}$ range was caused by the thermal decomposition of APTMS molecule.

Figure 6 reveals the changes in the surface chemistry of the nanoparticles upon consecutive functionalization steps during formation of the core-shell materials.

First, the successful formation of the $\text{TiO}_2@\text{SiO}_2$ particles was confirmed through the appearance of strong Si2p peak doublet at approx. 102.1 eV , which is typical for SiO_2 monolayer surface coverage on TiO_2 [57,58] (Figure 6a). The $\text{TiO}_2@\text{SiO}_2$ O1s reveals a complex nature, with multiple components characteristic for the SiO_2 (531.6 eV), TiO_2 (528.8 eV) and atomically mixed $\text{TiO}_2-\text{SiO}_2$ thin film (530.2 eV) [16,58], which are further modified by the presence of small amounts of adventitious carbon, carbonate and adsorbed water contamination resultant from the air exposure [59]. The observed SiO_2 :mixed: TiO_2 ratio was 9.2:3.5:1. The detailed information regarding the deconvolution with the proposed model is summarized in Table 1.

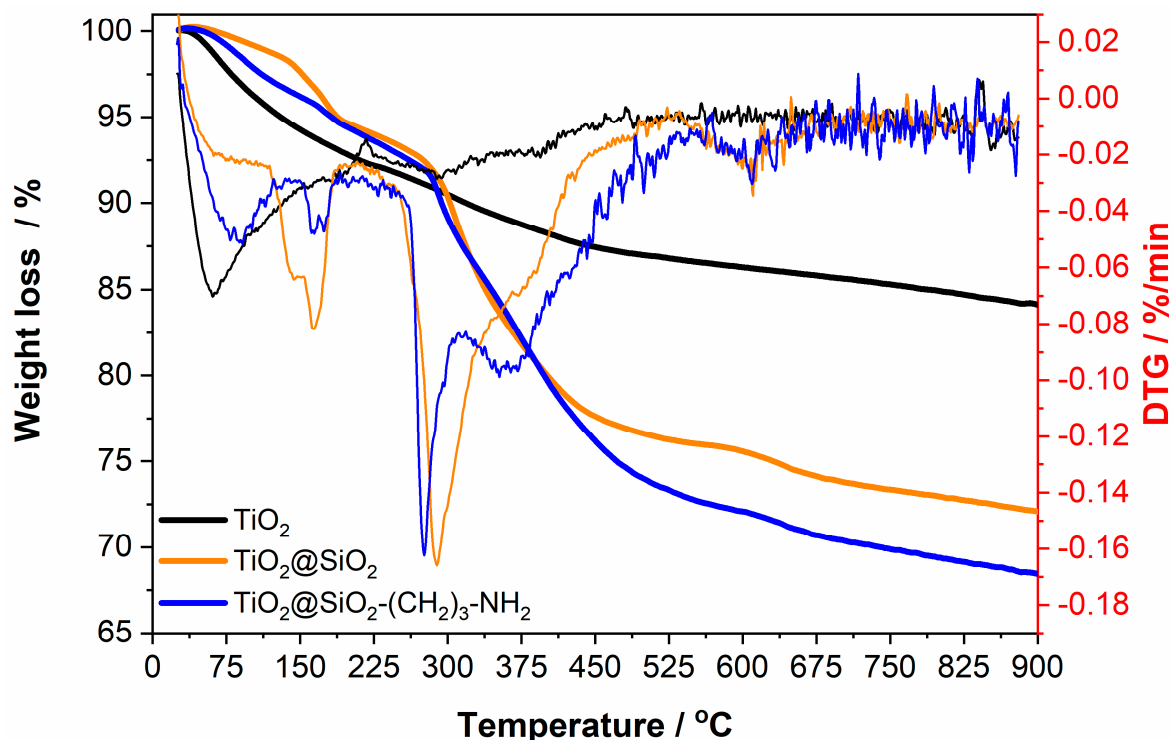


Figure 5. Thermogravimetric (TG) and thermogravimetric derivative (DTG) curves for TiO_2 , $\text{TiO}_2@SiO_2$ and $\text{TiO}_2@SiO_2-(CH_2)_3-NH_2$.

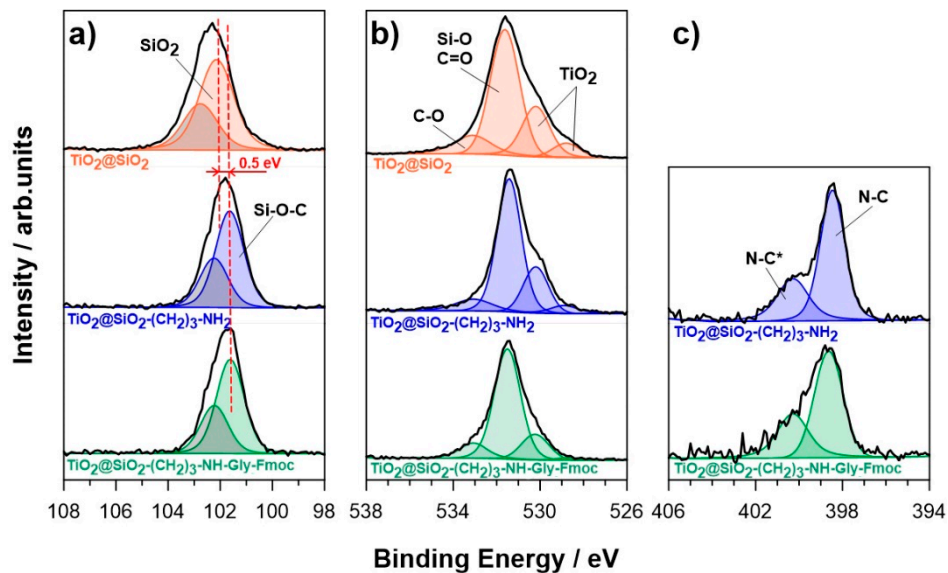


Figure 6. High-resolution XPS spectra for (a) $Si2p$, (b) $O1s$ and (c) $N1s$ recorded for each studied surface-modification and encapsulation step of $\text{TiO}_2@SiO_2$, together with the proposed deconvolution procedure.

Table 1. Distribution of Si, N, O and Ti chemical states, based on the Si2p, N1s, O1s and Ti2p high-resolution XPS spectral analyses with the proposed deconvolution model for each studied TiO₂@SiO₂ nanoparticle functionalization step.

		BE/eV	TiO ₂ @SiO ₂	TiO ₂ @SiO ₂ -(CH ₂) ₃ -NH ₂	TiO ₂ @SiO ₂ -(CH ₂) ₃ -NH-Gly-Fmoc
Si2p	SiO ₂	102.1	27	–	–
	Si-O-C	101.6	–	25.7	25.1
O1s	C-O, H ₂ O	533.1	7.2	5.4	6.4
	SiO ₂ , C=O	531.6	41.8	35.2	38.8
	SiO ₂ -TiO ₂	530.2	16.7	12.2	9.2
	TiO ₂	528.8	4.5	2.7	1.1
N1s	N-C	398.5	–	12.1	12.7
	N=C	400.3	–	5.8	6.7
Ti2p	TiO ₂	459.2	2.8	0.9	–

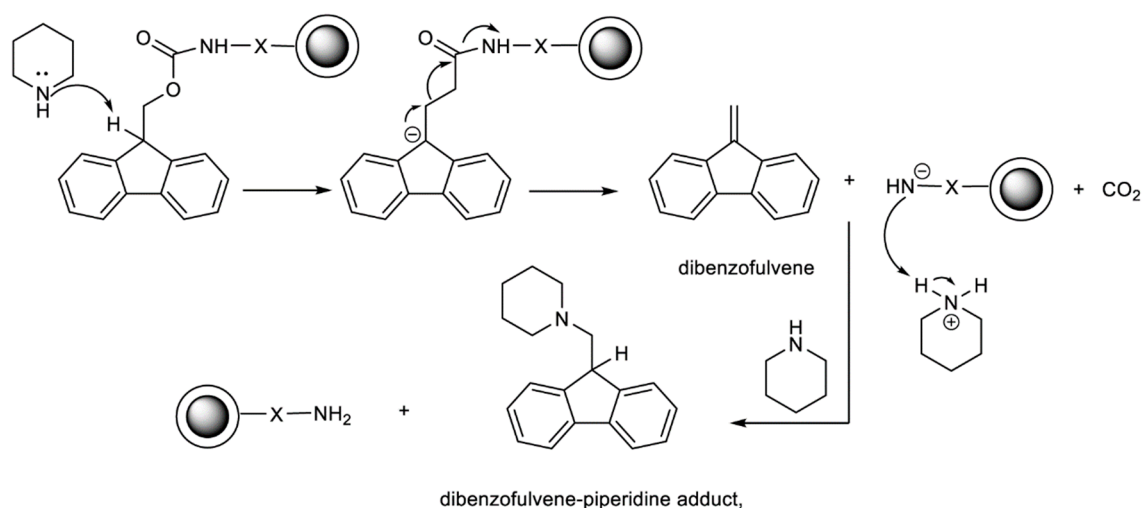
The consecutive functionalization of the core-shell TiO₂@SiO₂-(CH₂)₃-NH₂ with amino groups led to a negative shift of the Si2p peak doublet position by 0.5 eV due to the appearance of silicon oxycarbide Si-O-C interaction [60,61]. In parallel, the oxygen surface chemistry is significantly altered. The share of mixed TiO₂-SiO₂, SiO₂, and TiO₂ components drops approximately by a factor of 1.5. Last, but not least, a strong signal recorded in the N1s energy range revealed the presence of the amino -NH₂ species (398.5 eV) [62,63]. The N1s signal is characterized by a complex structure, with a second, two times smaller component, which may be the effect of NH₃⁺ protonation or deprotonation on NH-

Finally, the incorporation of Fmoc-glycine on the surface of encapsulated TiO₂@SiO₂ nanoparticles only slightly changed the chemistry, based on XPS analyses. Further decay in the O1s signal strength from titanium and silicon oxides was observed, except for the component located at 531.6 eV, which source next to SiO₂ is also C=O bonds in glycine [64,65]. Based on the XPS analyses of core level Si2p, O1s and N1s binding energy range (Figure 6a–c), the chemistry of SiO₂ and NH₂ species did not change significantly between TiO₂@SiO₂-(CH₂)₃-NH₂ and TiO₂@SiO₂-(CH₂)₃-NH-Gly-Fmoc nanoparticles. Moreover, the TiO₂ presence may no longer be recognized based on the Ti2p spectra.

2.3. Determination of Fmoc Group Loading on TiO₂@SiO₂-(CH₂)₃-NH-Gly-Fmoc Core-Shell Nanostructure

Nowadays, the solid-phase peptide synthesis using Fmoc/*t*-Bu method is one of the most frequent strategies to obtain a peptide. This method is applied for the peptide synthesis on a solid support with amino acid derivatives containing a base-labile Fmoc group protecting the amino group and acid-labile side chains [66]. Since there is a wide distribution of Fmoc amino acid derivatives, the peptide synthesis using this strategy is particularly cost-effective and does not require the usage of toxic hydrogen fluoride [67]. Fmoc group during synthesis is usually removed in a weak basic conditions, in 20% of piperidine in DMF. The reaction mechanism of Fmoc cleavage from solid support presented in Scheme 2 in the first step is based on β-elimination [68]. Initially, the proton from the fluorenyl group at the 9-position is removed by piperidine with the formation of dibenzofulvene Scheme 2. In the next step, the presence of piperidine causes the formation of dibenzofulvene-piperidine adducts based on the Michael-type addition [69]. This reaction usually occurs in electron-donor polar solvents, such as DMF.

The reaction of Fmoc protected core-shell and piperidine led to the formation of piperidine-dibenzofulvene adduct. Due to the fact that this adduct is soluble in reaction solvents, one can use the spectrophotometric measurement to determine the concentration of Fmoc groups based on Beer-Lambert law. The determination of Fmoc groups loading at core-shell nanostructure enable the calculation of the amino group prevalence at amino core-shell structure before the modification by Fmoc-Gly-OH.



Scheme 2. Mechanism of Fmoc group removal from solid support and formation of dibenzofulvene-piperidine adduct in the presence of piperidine.

In this work, we adopted the method previously invented for the determination of first anchored Fmoc-protected amino acids on resins to measure the presence of amino groups on the core-shell structure. Both mechanism and determination of molar absorption coefficient (ϵ) for piperidine-dibenzofulvene in different solutions have been reported in many studies. Therefore, we decided to calculate and compare the loading of Fmoc groups based on literature data using a different ϵ value both for core-shell structure, as well as for Fmoc-Gly-OH model sample.

The spectrophotometric measurements performed for both $\text{TiO}_2@\text{SiO}_2-(\text{CH}_2)_3\text{-NH-Gly-Fmoc}$ and Fmoc-Gly-OH are presented in Figure 7. In both graphs, two absorption maxima at 289 and 301-nm wavelengths are observed, corresponding to the presence of dibenzofulvene-piperidine adduct in the solution. The mechanism of the occurring reaction is presented in Scheme 2. The molar absorption coefficient (ϵ) was determined previously for this absorption maxima: ϵ (267 nm) = $17,500 \text{ dm}^3 \times \text{mol}^{-1} \times \text{cm}^{-1}$, ϵ (290 nm) = $5800 \text{ dm}^3 \times \text{mol}^{-1} \times \text{cm}^{-1}$ and ϵ (301 nm) $7800 \text{ dm}^3 \times \text{mol}^{-1} \times \text{cm}^{-1}$ in methylene chloride [70]. The similar value was also used for DMF solution: ϵ (266 nm) = $17,500 \text{ dm}^3 \times \text{mol}^{-1} \times \text{cm}^{-1}$, ϵ (289 nm) = $5800 \text{ dm}^3 \times \text{mol}^{-1} \times \text{cm}^{-1}$ and ϵ (300 nm) $7800 \text{ dm}^3 \times \text{mol}^{-1} \times \text{cm}^{-1}$ [71]. In many studies only one ϵ coefficient (301 nm) $7800 \text{ dm}^3 \times \text{mol}^{-1} \times \text{cm}^{-1}$ was used for the calculation of the loading of amino acids and other molecules on a resin [69,72–75].

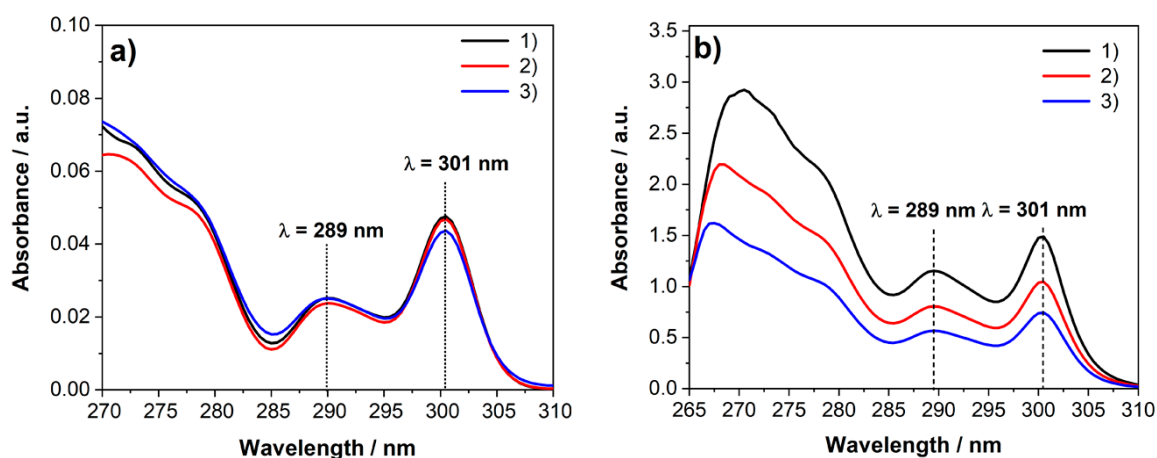


Figure 7. Absorption spectra with the concentrations in mol/dm^3 of (a) $\text{TiO}_2@\text{SiO}_2-(\text{CH}_2)_3\text{-NH-Gly-Fmoc}$, (b) Fmoc-Gly-OH used as the model sample.

Nevertheless, the detailed research on Fmoc-substituted resin at a different wavelength determined previously ($\epsilon = 6089 \text{ dm}^3 \times \text{mol}^{-1} \times \text{cm}^{-1}$) at 289,8 nm and ($\epsilon = 8021 \text{ dm}^3 \times \text{mol}^{-1} \times \text{cm}^{-1}$) at 301 nm [76] encouraged us to compare different ϵ coefficient of dibenzofulvene–piperidine in DMF for calculation of Fmoc groups on core-shell nanostructures and model sample (Fmoc–Gly–OH).

All measurements of adsorption spectra of dibenzofulvene–piperidine adduct were performed in triplicates. In the case of $\text{TiO}_2@\text{SiO}_2-(\text{CH}_2)_3\text{-NH-Gly-Fmoc}$ as well as Fmoc–Gly–OH, two absorption maxima were observed at 289 nm and 301 nm Figure 7. In both cases also the absorption band was observed at 267 nm, but due to the fact of intensity differences, this band was not included in the calculations of Fmoc loading. The detailed data of the maximum absorbance value for the examined materials are presented in Table 2.

Table 2. The absorbance maxima for $\text{TiO}_2@\text{SiO}_2-(\text{CH}_2)_3\text{-NH-Gly-Fmoc}$ and Fmoc–Gly–OH at 289 nm and 301 nm.

Sample	$\text{TiO}_2@\text{SiO}_2-(\text{CH}_2)_3\text{-NH-Gly-Fmoc}$			Fmoc–Gly–OH		
	m (mg)	A@289 nm	A@301 nm	m (mg)	A@289 nm	A@301 nm
(1)	2.06	0.025	0.048	0.25	1.15	1.49
(2)	2.06	0.024	0.047	0.17	0.81	1.03
(3)	2.08	0.025	0.044	0.11	0.57	0.74

The estimation of the Fmoc group (Z) loading on the $\text{TiO}_2@\text{SiO}_2-(\text{CH}_2)_3\text{-NH-Gly-Fmoc}$ core-shell nanostructure surface was calculated according to the equation presented in the Paragraph 3.4. The comparison of all calculated loadings of the Fmoc group for both examined materials is presented in Table 3. The obtained data directly indicate that in the case of $\text{TiO}_2@\text{SiO}_2-(\text{CH}_2)_3\text{-NH-Gly-Fmoc}$ the similar values of loading for Fmoc groups were obtained (6 $\mu\text{mol/g}$) taking into consideration the maximum band at $\lambda = 289 \text{ nm}$ and using both molar absorption coefficients: $\epsilon = 5800$ and $6089 \text{ dm}^3 \times \text{mol}^{-1} \times \text{cm}^{-1}$. The calculation performed for 301-nm wavelength confirmed the relation presented above. Conducted calculations gave the similar values of loading for Fmoc groups at the core-shell nanostructure of about 8 or 9 $\mu\text{mol/g}$ using molar absorption coefficient $\epsilon = 7800$ and $8021 \text{ dm}^3 \times \text{mol}^{-1} \times \text{cm}^{-1}$.

Table 3. Loading of Fmoc group (Z) for and Fmoc–Gly–OH calculated for 4 samples using a different value of molar absorption coefficient (ϵ).

ϵ ($\text{dm}^3 \times \text{mol}^{-1} \times \text{cm}^{-1}$)	$\text{TiO}_2@\text{SiO}_2-(\text{CH}_2)_3\text{-NH-Gly-Fmoc}$		Fmoc–Gly–OH	
	Z@289 nm ($\mu\text{mol/g}$)	Z@ 301 nm ($\mu\text{mol/g}$)	Z@289 nm (mmol/g)	Z@ 301 nm (mmol/g)
5800	6.3; 6.0; 6.2	–	2.38; 2.46; 2.68	–
7800	–	9.0;8.8;8.1	–	2.29; 2.33; 2.58
6089	6.0; 5.7; 5.9	–	2.27; 2.35; 2.55	–
8021	–	8.7; 8.5; 7.9	–	2.23; 2.27; 2.52

The differences in the given calculations of Fmoc group loading probably decrease with the increasing mass of $\text{TiO}_2@\text{SiO}_2-(\text{CH}_2)_3\text{-NH-Gly-Fmoc}$ samples used for a measurement.

In the case of Fmoc group presence determination for Fmoc–Gly–OH in the solution used as the model sample, our calculation is almost the same regardless of the intensity of absorption band both at 289 nm, as well as 301 nm. The concentration of the Fmoc group was obtained at the level of 2 mmol/g.

The calculation of Fmoc-group loading at solid materials described in this work provides the information on how many active amino groups are present at these materials before modifications. The presented method is much simpler and cost-effective in comparison with the commonly used methods for amino groups determination. Additionally, presented method can be adopted for the characterization of nanomaterials.

3. Materials and Methods

3.1. Materials

All reagents and solvents were of analytical grade and used without purification. Sodium dodecyl sulfate (SDS), titanium (IV) isopropoxide (TTIP), sodium citrate dihydrate, tetraethyl orthosilicate (TEOS), 3-(aminopropyl)trimethoxysilane (APTMS), Fmoc-glycine (Fmoc-Gly-OH) used as a control sample, piperidine, *N,N'*-diisopropylcarbodiimide (DIC), 4-dimethylaminopyridine (DMAP) and tetrachloro-*p*-benzoquinone (*p*-chloranil) were purchased from Sigma-Aldrich (Poznan, Poland).

3.2. Synthesis of TiO₂ Derivatives

3.2.1. Synthesis of TiO₂

Titanium precursor (TTIP) (9.678 g, 33.7 mmol) was added to 200 mL of 8-mmol/L SDS dissolved in water. The reaction mixture was stirred for 1 h in 90 °C until white precipitate was obtained. Subsequently, the obtained product was separated by centrifugation, washed with distilled water until complete removal of SDS and the dried on air.

3.2.2. Synthesis of TiO₂@SiO₂

TiO₂ (50 mg, 6.25 mmol) obtained in the procedure mentioned above was added to 100 mL of ethanol solution containing 30 mg of sodium citrate. The solution was vigorously stirred on magnetic stirrer and adjusted to pH = 9 using ammonia hydroxide. Then, 10 mL (44.83 mmol) of tetraethyl orthosilicate (TEOS) was added to the reaction mixture. After stirring for 24 h, the obtained white precipitate was collected by centrifugation, washed with ethanol and dried.

3.2.3. Synthesis of TiO₂@SiO₂-(CH₂)₃-NH₂

TiO₂@SiO₂ (100 mg) and 3-(aminopropyl)trimethoxysilane (APTMS; 0.7 mL, 4.00 mmol) were dissolved in 1.5 mL of toluene. Subsequently, the solution was transferred to a round-bottomed flask equipped with a reflux condenser and stirred at 120 °C for 24 h. The reaction mixture was cooled down to the room temperature, the obtained particulate was washed with diethyl ether and dichloromethane and dried in a stream of nitrogen. The effectiveness of the amination reaction was confirmed based on the chloranil test [45].

3.2.4. Synthesis of TiO₂@SiO₂-(CH₂)₃-NH-Gly-Fmoc

The mixture of TiO₂@SiO₂-(CH₂)₃-NH₂ (40 mg) and Fmoc-glycine (Fmoc-Gly-OH) (10 mg, 0.0336 mmol) dissolved in methylene chloride: DMF, 1:1, (*v/v*) was cooled in an ice-bath to 0 °C. Then, 50 µL of *N,N'*-diisopropylcarbodiimide (DIC) and 0.5 mg of 4-dimethylaminopyridine (DMAP) were added to the solution and stirred overnight. After this time, the resulting residue was centrifuged and washed several times with DMF and dichloromethane until the absence of substrates. Obtained residue was dried in vacuum desiccator over P₂O₅ for 12 h at room temperature, resulting in 31 mg of the desired product.

3.3. Material Characterization

Transmission electron microscope (TEM) images were obtained on Tecnai G2 Spirit BioTWIN by FEI (Eindhoven, the Netherlands). Scanning electron microscopy (SEM) images were obtained on Hitachi S-3400N scanning electron microscope. Fourier-transform infrared spectroscopy (FT-IR) analyses were carried out using Bruker IFS 66 Spectrometer (Ettlingen, Germany).

The thermal analysis of the nanostructures was measured using Jupiter STA 449 F3 thermogravimetry connected to the QMS 403 C quadrupole mass spectrometer (Netzsch, Selb, Germany). The measurements were carried out in an inert gas (argon) atmosphere, from room temperature to 1000 °C, with a heating rate of 10 °C/min.

X-ray photoelectron spectroscopy (XPS) studies were carried out on PHI QUANTERA II spectrometer. The spectroscope is equipped with monochromatic AlK α source, the analyses were carried out with a spot diameter of 250 μm and in the binding energy range of C1s, O1s, N1s, Si2p and Ti2p spectra. Measurements were conducted with 20 eV pass energy, with the charge compensation controlled through low-energy electron and Ar⁺ ions flow by a flood gun.

The spectrophotometric measurements were determined by using UV-vis spectrophotometer, Perkin Elmer, Lambda 650 model (Shelton, CT, USA). The measurement was performed at 298 K using 1-cm-thick quartz spectrophotometric cuvettes in 20% (*v/v*) solution of piperidine in DMF at the 200–800 nm wavelength range.

3.4. The Procedure of Amino Group Loading on Nanoparticles

The dibenzofulvene–piperidine adducts is usually soluble in the reaction solvent. The occurrence of dibenzofulvene–piperidine in the solution after cleavage with piperidine gives the possibility to use the absorbance spectroscopy. This method is utilized to calculate the number of amino groups in the case of amino acid derivatives or surface coverage by amino groups in the case of NPs derivatives containing amino groups protected by Fmoc groups. In this work, we adopted the spectrophotometric measurements to determine the concentration of amino groups at the TiO₂ NPs modified by Fmoc–Gly–OH derivative (TiO₂@SiO₂–(CH₂)₃–NH–Gly–Fmoc). Additionally, we calculated the amount of amino groups for Fmoc–Gly–OH used as a model sample according to the procedure described below.

About 2 mg of TiO₂@SiO₂–(CH₂)₃–NH–Gly–Fmoc sample Table 2 was weighted in a spectrophotometric quartz cuvette. Then, 3 mL of 20% (*v/v*) piperidine in DMF was added and the suspension was stirred for 20 min. After this time, the precipitate was left for 1 h to settle down at the bottom of the cuvette and then the absorption spectra were obtained. The estimation of the Fmoc group loading was conducted according to the equation [76]. The knowledge concerning the loading of Fmoc groups attached to NPs enables the estimation of amino groups load at the nanoparticle surface.

$$Z = \frac{A \times v}{\epsilon \times m \times l} \quad (1)$$

Z—Fmoc group loading (mol/g)

A—Absorbance value at the maximum absorption (nm)

v—Volume of solvent (dm³)

ϵ —Molar absorption coefficient (dm³ × mol^{−1} × cm^{−1} maximum absorption)

m—Sample weight (mg)

l—Length of the cell (1 cm)

4. Conclusions

In this study, the synthesis of TiO₂, TiO₂@SiO₂, TiO₂@SiO₂–(CH₂)₃–NH₂ core-shell structures was presented. The Fmoc–glycine (Fmoc–Gly–OH) was used as a modification agent of TiO₂@SiO₂–(CH₂)₃–NH₂ to obtain TiO₂@SiO₂–(CH₂)₃–NH–Gly–Fmoc. All the obtained nanostructures were described using various analytical methods: transmission electron microscopy (TEM), Fourier-transform infrared spectroscopy (FTIR), thermogravimetric analysis (TGA) and X-ray photoelectron spectroscopy (XPS). Additionally, all of these measurements confirmed the effectiveness of each modification step. The deposition of Fmoc–glycine (Fmoc–Gly–OH) on the core-shell structure was used to develop the method for quantitative determination of Fmoc groups present at newly obtained materials. In this procedure, (Fmoc) groups were cleaved using 20% (*v/v*) solution of piperidine in DMF. This reaction leads to the formation of dibenzofulvene–piperidine adduct enabling the estimation of Fmoc groups loading by UV-vis spectroscopy. The comparison of different molar absorption coefficients—5800 and 6089 dm³ × mol^{−1} × cm^{−1} and 7800 and 8021 dm³ × mol^{−1} × cm^{−1}

was used to calculate the loading of Fmoc groups at 289 nm and 301 nm, respectively. Furthermore, the presence of Fmoc groups in solution was calculated for Fmoc–Gly–OH used as the model sample. The described methodology is particularly useful for the determination of the number of amino groups in various nanomaterials.

Author Contributions: Conceptualization, E.S. and P.N. methodology, E.S.; P.N.; J.R. formal analysis, E.S.; P.N.; B.G.; J.R.; investigation, E.S.; B.G.; P.N.; J.R.; A.K. writing—original draft preparation, E.S.; P.N.; B.G.; J.R. writing—review and editing, E.S.; P.N.; B.G.; J.R.; T.O.; A.K. visualization, E.S.; P.N.; supervision, P.N.; B.G.; J.R.; T.O. All authors have read and agreed to the published version of the manuscript.

Funding: This research project was supported by the University of Gdansk supporting young scientists and PhD students (grant No. BMN 539-T050-B465-20) (E.S.).

Conflicts of Interest: The authors declare no conflict of interest.

References

1. Lewkowicz, A.; Synak, A.; Grobelna, B.; Bojarski, P.; Bogdanowicz, R.; Karczewski, J.; Szczodrowski, K.; Behrendt, M. Thickness and structure change of titanium(IV) oxide thin films synthesized by the sol–gel spin coating method. *Opt. Mater.* **2014**, *36*, 1739–1744. [[CrossRef](#)]
2. Wang, Y.; Sun, C.; Zhao, X.; Cui, B.; Zeng, Z.; Wang, A.; Liu, G.; Cui, H. The Application of Nano-TiO₂ Photo Semiconductors in Agriculture. *Nanoscale Res. Lett.* **2016**, *11*, 529. [[CrossRef](#)] [[PubMed](#)]
3. Lewkowicz, A.; Bojarski, P.; Synak, A.; Grobelna, B.; Akopova, I.; Gryczyński, I.; Kułak, L. Concentration-Dependent Fluorescence Properties of Rhodamine 6G in Titanium Dioxide and Silicon Dioxide Nanolayers. *J. Phys. Chem. C* **2012**, *116*, 12304–12311. [[CrossRef](#)]
4. Synak, A.; Bojarski, P.; Grobelna, B.; Kułak, L.; Szczepańska, E.; Mońka, M. Concentration—Dependent fluorescence properties of Nile Red in TiO₂ based thin films. *J. Mol. Liq.* **2020**, *306*. [[CrossRef](#)]
5. Mahltig, B.; Böttcher, H.; Rauch, K.; Dieckmann, U.; Nitsche, R.; Fritz, T. Optimized UV protecting coatings by combination of organic and inorganic UV absorbers. *Thin Solid Films* **2005**, *1–2*, 108–114. [[CrossRef](#)]
6. Liu, S.; Zhang, N.; Tang, Z.-R.; Xu, Y.-J. Synthesis of One-Dimensional CdS@TiO₂ Core–Shell Nanocomposites Photocatalyst for Selective Redox: The Dual Role of TiO₂ Shell. *ACS Appl. Mater. Interfaces* **2012**, *4*, 6378–6385. [[CrossRef](#)]
7. Szczepańska, E.; Bielicka-Giełdoń, A.; Niska, K.; Strankowska, J.; Żebrowska, J.; Inkiewicz-Stepniak, I.; Łubkowska, B.; Sweboccki, T.; Skowron, P.; Grobelna, B. Synthesis of silver nanoparticles in context of their cytotoxicity, antibacterial activities, skin penetration and application in skincare products. *Supramol. Chem.* **2020**, *32*, 207–221. [[CrossRef](#)]
8. Synak, A.; Szczepańska, E.; Grobelna, B.; Gondek, J.; Mońka, M.; Gryczynski, I.; Bojarski, P. Photophysical properties and detection of Valrubicin on plasmonic platforms. *Dyes Pigment.* **2019**, *163*, 623–627. [[CrossRef](#)]
9. Baranowska-Wójcik, E.; Sz wajgier, D.; Oleszczuk, P.; Winiarska-Mieczan, A. Effects of Titanium Dioxide Nanoparticles Exposure on Human Health—A Review. *Biol. Trace Elem. Res.* **2020**, *193*, 118–129. [[CrossRef](#)]
10. Zhang, X.; Niu, H.; Pan, Y.; Shi, Y.; Cai, Y. Modifying the surface of Fe₃O₄/SiO₂ magnetic nanoparticles with C18/NH₂ mixed group to get an efficient sorbent for anionic organic pollutants. *J. Colloid Interface Sci.* **2011**, *362*, 107–112. [[CrossRef](#)]
11. Ta, T.K.H.; Trinh, M.-T.; Long, N.V.; Nguyen, T.T.M.; Nguyen, T.L.T.; Thuoc, T.L.; Phan, B.T.; Mott, D.; Maenosono, S.; Tran-Van, H.; et al. Synthesis and surface functionalization of Fe₃O₄-SiO₂ core-shell nanoparticles with 3-glycidoxypropyltrimethoxysilane and 1,1'-carbonyldiimidazole for bio-applications. *Colloids Surf. A Physicochem. Eng. Asp.* **2016**, *504*, 376–383. [[CrossRef](#)]
12. Roto, R.; Yusran, Y.; Kuncaka, A. Magnetic adsorbent of Fe₃O₄@SiO₂ core-shell nanoparticles modified with thiol group for chlorauric ion adsorption. *Appl. Surf. Sci.* **2016**, *377*, 30–36. [[CrossRef](#)]
13. Zhang, S.; Zhang, Y.; Liu, J.; Xu, Q.; Xiao, H.; Wang, X.; Xu, H.; Zhou, J. Thiol modified Fe₃O₄@SiO₂ as a robust, high effective, and recycling magnetic sorbent for mercury removal. *Chem. Eng. J.* **2013**, *226*, 30–38. [[CrossRef](#)]
14. Marchant, M.J.; Guzmán, L.; Corvalán, A.H.; Kogan, M.J. Gold@Silica Nanoparticles Functionalized with Oligonucleotides: A Prominent Tool for the Detection of the Methylated Reprimo Gene in Gastric Cancer by Dynamic Light Scattering. *Nanomaterials* **2019**, *9*, 1333. [[CrossRef](#)]

15. Teng, Y.; Jiang, C.; Ruotolo, A.; Pong, P.W.T. Amine-Functionalized Fe₂O₃-SiO₂ Core-Shell Nanoparticles with Tunable Sizes. *IEEE Trans. Nanotechnol.* **2018**, *17*, 69–77. [CrossRef]
16. Kulpa, A.; Ryl, J.; Skowierzak, G.; Koterwa, A.; Schroeder, G.; Ossowski, T.; Niedziałkowski, P. Comparison of Cadmium Cd²⁺ and Lead Pb²⁺ Binding by Fe₂O₃@SiO₂-EDTA Nanoparticles—Binding Stability and Kinetic Studies. *Electroanalysis* **2020**, *32*, 588–597. [CrossRef]
17. Xu, X.; Sun, Y.; Zhang, Q.; Cai, H.; Li, Q.; Zhou, S. Synthesis and photocatalytic activity of plasmon-enhanced core-shell upconversion luminescent photocatalytic Ag@SiO₂@YF₃:Ho³⁺@TiO₂ nanocomposites. *Opt. Mater.* **2019**, *94*, 444–453. [CrossRef]
18. Liu, H.; Lin, C.; Ma, Z.; Yu, H.; Zhou, S. Gold Nanoparticles on Mesoporous SiO₂-Coated Magnetic Fe₃O₄ Spheres: A Magnetically Separatable Catalyst with Good Thermal Stability. *Molecules* **2013**, *18*, 14258–14267. [CrossRef]
19. Cheng, F.; Sajedin, S.M.; Kelly, S.M.; Lee, A.F.; Kornherr, A. UV-stable paper coated with APTES-modified P25 TiO₂ nanoparticles. *Carbohydr. Polym.* **2014**, *114*, 246–252. [CrossRef]
20. Kulpa, A.; Ryl, J.; Schroeder, G.; Koterwa, A.; Sein Anand, J.; Ossowski, T.; Niedziałkowski, P. Simultaneous voltammetric determination of Cd²⁺, Pb²⁺, and Cu²⁺ ions captured by Fe₃O₄@SiO₂ core-shell nanostructures of various outer amino chain length. *J. Mol. Liq.* **2020**, *314*, 113677. [CrossRef]
21. Kyaw, H.H.; Al-Harhi, S.H.; Sellai, A.; Dutta, J. Self-organization of gold nanoparticles on silanated surfaces. *Beilstein J. Nanotechnol.* **2015**, *6*, 2345–2353. [CrossRef] [PubMed]
22. Masitas, R.A.; Khachian, I.V.; Bill, B.L.; Zamborini, F.P. Effect of Surface Charge and Electrode Material on the Size-Dependent Oxidation of Surface-Attached Metal Nanoparticles. *Langmuir* **2014**, *30*, 13075–13084. [CrossRef] [PubMed]
23. Qin, M.; Hou, S.; Wang, L.; Feng, X.; Wang, R.; Yang, Y.; Wang, C.; Yu, L.; Shao, B.; Qiao, M. Two methods for glass surface modification and their application in protein immobilization. *Colloids Surf. B Biointerfaces* **2007**, *60*, 243–249. [CrossRef] [PubMed]
24. Kim, H.; Kwon, J.-Y. Enzyme immobilization on metal oxide semiconductors exploiting amine functionalized layer. *RSC Adv.* **2017**, *7*, 19656–19661. [CrossRef]
25. Vashist, S.K.; Lam, E.; Hrapovic, S.; Male, K.B.; Luong, J.H.T. Immobilization of Antibodies and Enzymes on 3-Aminopropyltriethoxysilane-Functionalized Bioanalytical Platforms for Biosensors and Diagnostics. *Chem. Rev.* **2014**, *114*, 11083–11130. [CrossRef]
26. Gunda, N.S.K.; Singh, M.; Norman, L.; Kaur, K.; Mitra, S.K. Optimization and characterization of biomolecule immobilization on silicon substrates using (3-aminopropyl)triethoxysilane (APTES) and glutaraldehyde linker. *Appl. Surf. Sci.* **2014**, *305*, 522–530. [CrossRef]
27. Son, J.; Kim, J.; Lee, K.; Hwang, J.; Choi, Y.; Seo, Y.; Jeon, H.; Kang, H.C.; Woo, H.-M.; Kang, B.-J.; et al. DNA aptamer immobilized hydroxyapatite for enhancing angiogenesis and bone regeneration. *Acta Biomater.* **2019**, *99*, 469–478. [CrossRef]
28. Ruiz-Cañas, M.C.; Corredor, L.M.; Quintero, H.I.; Manrique, E.; Romero Bohórquez, A.R. Morphological and Structural Properties of Amino-Functionalized Fumed Nanosilica and Its Comparison with Nanoparticles Obtained by Modified Stöber Method. *Molecules* **2020**, *25*, 2868. [CrossRef]
29. Howarter, J.A.; Youngblood, J.P. Optimization of Silica Silanization by 3-Aminopropyltriethoxysilane. *Langmuir* **2006**, *22*, 11142–11147. [CrossRef]
30. Yamaura, M.; Camilo, R.L.; Sampaio, L.C.; Macêdo, M.A.; Nakamura, M.; Toma, H.E. Preparation and characterization of (3-aminopropyl)triethoxysilane-coated magnetite nanoparticles. *J. Magn. Magn. Mater.* **2004**, *279*, 210–217. [CrossRef]
31. Asenath Smith, E.; Chen, W. How To Prevent the Loss of Surface Functionality Derived from Aminosilanes. *Langmuir* **2008**, *24*, 12405–12409. [CrossRef] [PubMed]
32. Jung, H.-S.; Moon, D.-S.; Lee, J.-K. Quantitative Analysis and Efficient Surface Modification of Silica Nanoparticles. Available online: <https://www.hindawi.com/journals/jnm/2012/593471/> (accessed on 3 July 2020).
33. Kralj, S.; Drogenik, M.; Makovec, D. Controlled surface functionalization of silica-coated magnetic nanoparticles with terminal amino and carboxyl groups. *J. Nanopart. Res.* **2011**, *13*, 2829–2841. [CrossRef]
34. Kunc, F.; Balhara, V.; Brinkmann, A.; Sun, Y.; Leek, D.M.; Johnston, L.J. Quantification and Stability Determination of Surface Amine Groups on Silica Nanoparticles Using Solution NMR. *Anal. Chem.* **2018**, *90*, 13322–13330. [CrossRef] [PubMed]

35. Čampelj, S.; Makovec, D.; Drogenik, M. Functionalization of magnetic nanoparticles with 3-aminopropyl silane. *J. Magn. Magn. Mater.* **2009**, *321*, 1346–1350. [[CrossRef](#)]
36. Morozov, R.; Avdin, V.; Krivtsov, I.; Gorshkov, A.; Urzhumova, A.; Osinskaya, A.; Yuzhalkin, D. Modification with Amino Groups of Composite SiO₂–TiO₂ and Pure TiO₂ Spheres Prepared via the Peroxo Route. *Chem* **2018**, *10*, 24–36. [[CrossRef](#)]
37. Torelli, M.D.; Putans, R.A.; Tan, Y.; Lohse, S.E.; Murphy, C.J.; Hamers, R.J. Quantitative Determination of Ligand Densities on Nanomaterials by X-ray Photoelectron Spectroscopy. *ACS Appl. Mater. Interfaces* **2015**, *7*, 1720–1725. [[CrossRef](#)]
38. Hennig, A.; Borchering, H.; Jaeger, C.; Hatami, S.; Würth, C.; Hoffmann, A.; Hoffmann, K.; Thiele, T.; Schedler, U.; Resch-Genger, U. Scope and Limitations of Surface Functional Group Quantification Methods: Exploratory Study with Poly(acrylic acid)-Grafted Micro- and Nanoparticles. *J. Am. Chem. Soc.* **2012**, *134*, 8268–8276. [[CrossRef](#)]
39. Li, W.; Zhao, D. Extension of the Stöber Method to Construct Mesoporous SiO₂ and TiO₂ Shells for Uniform Multifunctional Core–Shell Structures. *Adv. Mater.* **2013**, *25*, 142–149. [[CrossRef](#)]
40. Yuenyongsuwan, J.; Nithiyakorn, N.; Sabkird, P.; O’Rear, E.A.; Pongprayoon, T. Surfactant effect on phase-controlled synthesis and photocatalyst property of TiO₂ nanoparticles. *Mater. Chem. Phys.* **2018**, *214*, 330–336. [[CrossRef](#)]
41. Stöber, W.; Fink, A.; Bohn, E. Controlled growth of monodisperse silica spheres in the micron size range. *J. Colloid Interface Sci.* **1968**, *26*, 62–69. [[CrossRef](#)]
42. Nozawa, K.; Gailhanou, H.; Raison, L.; Panizza, P.; Ushiki, H.; Sellier, E.; Delville, J.P.; Delville, M.H. Smart Control of Monodisperse Stöber Silica Particles: Effect of Reactant Addition Rate on Growth Process. *Langmuir* **2005**, *21*, 1516–1523. [[CrossRef](#)] [[PubMed](#)]
43. Kang, J.; Li, Y.; Chen, Y.; Wang, A.; Yue, B.; Qu, Y.; Zhao, Y.; Chu, H. Core–shell Ag@SiO₂ nanoparticles of different silica shell thicknesses: Preparation and their effects on photoluminescence of lanthanide complexes. *Mater. Res. Bull.* **2015**, *71*, 116–121. [[CrossRef](#)]
44. Kamarudin, N.H.N.; Jalil, A.A.; Triwahyono, S.; Salleh, N.F.M.; Karim, A.H.; Mukti, R.R.; Hameed, B.H.; Ahmad, A. Role of 3-aminopropyltriethoxysilane in the preparation of mesoporous silica nanoparticles for ibuprofen delivery: Effect on physicochemical properties. *Microporous Mesoporous Mater.* **2013**, *180*, 235–241. [[CrossRef](#)]
45. Thorkild, C. A qualitative test for monitoring coupling completeness in solid phase peptide synthesis using chloranil. *Acta Chem. Scand. B* **1979**, *33*, 763–766. [[CrossRef](#)]
46. Jia, C.; Qi, W.; He, Z.; Yang, H.; Qiao, B. Synthesis of heptapeptides and analysis of sequence by tandem ion trap mass spectrometry. *Cent. Eur. J. Chem.* **2006**, *4*, 285–298. [[CrossRef](#)]
47. Czapryniak, J.; Niedziałkowski, P.; Karbarz, M.; Ossowski, T.; Stojek, Z. Lysine and Arginine Oligopeptides Tagged with Anthraquinone: Electrochemical Properties. *Electroanalysis* **2012**, *24*, 975–982. [[CrossRef](#)]
48. Ullah, S.; Ferreira-Neto, E.P.; Pasa, A.A.; Alcântara, C.C.J.; Acuña, J.J.S.; Bilmes, S.A.; Martínez Ricci, M.L.; Landers, R.; Fermiro, T.Z.; Rodrigues-Filho, U.P. Enhanced photocatalytic properties of core@shell SiO₂@TiO₂ nanoparticles. *Appl. Catal. B Environ.* **2015**, *179*, 333–343. [[CrossRef](#)]
49. Bai, Y.; Li, Z.; Cheng, B.; Zhang, M.; Su, K. Higher UV-shielding ability and lower photocatalytic activity of TiO₂@SiO₂/APTES and its excellent performance in enhancing the photostability of poly(p-phenylene sulfide). *RSC Adv.* **2017**, *7*, 21758–21767. [[CrossRef](#)]
50. Panwar, K.; Jassal, M.; Agrawal, A.K. TiO₂–SiO₂ Janus particles with highly enhanced photocatalytic activity. *RSC Adv.* **2016**, *6*, 92754–92764. [[CrossRef](#)]
51. León, A.; Reuquen, P.; Garín, C.; Segura, R.; Vargas, P.; Zapata, P.; Orihuela, P.A. FTIR and Raman Characterization of TiO₂ Nanoparticles Coated with Polyethylene Glycol as Carrier for 2-Methoxyestradiol. *Appl. Sci.* **2017**, *7*, 49. [[CrossRef](#)]
52. Huang, C.; Bai, H.; Huang, Y.; Liu, S.; Yen, S.; Tseng, Y. Synthesis of Neutral/Hydrosol and Its Application as Antireflective Self-Cleaning Thin Film. *Int. J. Photoenergy* **2012**, *2012*, 1–8. [[CrossRef](#)]
53. Fatimah, I.; Prakoso, N.I.; Sahroni, I.; Musawwa, M.M.; Sim, Y.-L.; Kooli, F.; Muraza, O. Physicochemical characteristics and photocatalytic performance of TiO₂/SiO₂ catalyst synthesized using biogenic silica from bamboo leaves. *Heliyon* **2019**, *5*, e02766. [[CrossRef](#)] [[PubMed](#)]

54. Li, S.; Ma, W.; Zhou, Y.; Chen, X.; Ma, M.; Xu, Y.; Ding, Z.; Wu, X. 3-aminopropyltriethoxysilanes Modified Porous Silicon as a Voltammetric Sensor for Determination of Silver Ion. *Int. J. Electrochem. Sci.* **2013**, *8*, 12.
55. Pretsch, E.; Bühlmann, P.; Badertscher, M. *Structure Determination of Organic Compounds*; Springer: Berlin/Heidelberg, Germany, 2009; ISBN 978-3-540-93809-5.
56. Zhao, J.; Milanova, M.; Warmoeskerken, M.; Dutschk, V. Surface modification of TiO₂ nanoparticles with silane coupling agents. *Colloid Surf. A* **2012**, *413*, 273–279. [[CrossRef](#)]
57. Abad, J.; Gonzalez, C.; de Andres, P.L.; Roman, E. Characterization of thin silicon overlayers on rutileTiO₂(110)–(1×1). *Phys. Rev. B* **2010**, *82*, 165420. [[CrossRef](#)]
58. Ondračka, P.; Nečas, D.; Carette, M.; Elisabeth, S.; Holec, D.; Granier, A.; Goulet, A.; Zajíčková, L.; Richard-Plouet, M. Unravelling local environments in mixed TiO₂–SiO₂ thin films by XPS and ab initio calculations. *Appl. Surf. Sci.* **2020**, *510*, 145056. [[CrossRef](#)]
59. Barr, T.L.; Seal, S. Nature of the use of adventitious carbon as a binding energy standard. *J. Vac. Sci. Technol. A* **1995**, *13*, 1239–1246. [[CrossRef](#)]
60. Önnby, C.; Pantano, C.G. Silicon oxycarbide formation on SiC surfaces and at the SiC/SiO₂ interface. *J. Vac. Sci. Technol. A* **1997**, *15*, 1597–1602. [[CrossRef](#)]
61. Kaur, A.; Chahal, P.; Hogan, T. Selective Fabrication of SiC/Si Diodes by Excimer Laser Under Ambient Conditions. *IEEE Electron Device Lett.* **2016**, *37*, 142–145. [[CrossRef](#)]
62. Niedziałkowski, P.; Bogdanowicz, R.; Zięba, P.; Wysocka, J.; Ryl, J.; Sobaszek, M.; Ossowski, T. Melamine-modified Boron-doped Diamond towards Enhanced Detection of Adenine, Guanine and Caffeine. *Electroanalysis* **2016**, *28*, 211–221. [[CrossRef](#)]
63. Bogdanowicz, R.; Sawczak, M.; Niedzialkowski, P.; Zieba, P.; Finke, B.; Ryl, J.; Karczewski, J.; Ossowski, T. Novel Functionalization of Boron-Doped Diamond by Microwave Pulsed-Plasma Polymerized Allylamine Film. *J. Phys. Chem. C* **2014**, *118*, 8014–8025. [[CrossRef](#)]
64. Calborean, A.; Martin, F.; Marconi, D.; Turcu, R.; Kacso, I.E.; Buimaga-Iarinca, L.; Graur, F.; Turcu, I. Adsorption mechanisms of L-Glutathione on Au and controlled nano-patterning through Dip Pen Nanolithography. *Mater. Sci. Eng. C Mater. Biol. Appl.* **2015**, *57*, 171–180. [[CrossRef](#)] [[PubMed](#)]
65. Wysocka, J.; Ciešlik, M.; Krakowiak, S.; Ryl, J. Carboxylic acids as efficient corrosion inhibitors of aluminium alloys in alkaline media. *Electrochim. Acta* **2018**, *289*, 175–192. [[CrossRef](#)]
66. Zinieris, N.; Leondiadis, L.; Ferderigos, N. N α -Fmoc Removal from Resin-Bound Amino Acids by 5% Piperidine Solution. *J. Comb. Chem.* **2005**, *7*, 4–6. [[CrossRef](#)] [[PubMed](#)]
67. Behrendt, R.; White, P.; Offer, J. Advances in Fmoc solid-phase peptide synthesis. *J. Pept. Sci.* **2016**, *22*, 4–27. [[CrossRef](#)]
68. Luna, O.F.; Gomez, J.; Cárdenas, C.; Albericio, F.; Marshall, S.H.; Guzmán, F. Deprotection Reagents in Fmoc Solid Phase Peptide Synthesis: Moving Away from Piperidine? *Molecules* **2016**, *21*, 1542. [[CrossRef](#)]
69. Vergel Galeano, C.F.; Rivera Monroy, Z.J.; Rosas Pérez, J.E.; García Castañeda, J.E. Efficient Synthesis of Peptides with 4-Methylpiperidine as Fmoc Removal Reagent by Solid Phase Synthesis. *J. Mex. Chem. Soc.* **2014**, *58*, 386–392.
70. Meienhofer, J.; Waki, M.; Heimre, E.P.; Lambros, T.J.; Makofske, R.C.; Chang, C.-D. Solid Phase Synthesis Without Repetitive Acidolysis. *Int. J. Pept. Protein Res.* **1979**, *13*, 35–42. [[CrossRef](#)]
71. Seebach, D.; Schreiber, J.V.; Abele, S.; Daura, X.; van Gunsteren, W.F. Structure and Conformation of β -Oligopeptide Derivatives with Simple Proteinogenic Side Chains: Circular Dichroism and Molecular Dynamics Investigations. *Helv. Chim. Acta* **2000**, *83*, 34–57. [[CrossRef](#)]
72. Zarra, R.; Montesarchio, D.; Coppola, C.; Bifulco, G.; Di Micco, S.; Izzo, I.; De Riccardis, F. Design, Synthesis, and Hybridisation of Water-Soluble, Peptoid Nucleic Acid Oligomers Tagged with Thymine. *Eur. J. Org. Chem.* **2009**, *2009*, 6113–6120. [[CrossRef](#)]
73. Carbajo, D.; El-Faham, A.; Royo, M.; Albericio, F. Optimized Stepwise Synthesis of the API Liraglutide Using BAL Resin and Pseudoprolines. *ACS Omega* **2019**, *4*, 8674–8680. [[CrossRef](#)]
74. Ziegler, T.; Schips, C. An efficient Mitsunobu protocol for the one-pot synthesis of S-glycosyl amino-acid building blocks and their use in combinatorial spot synthesis of glycopeptide libraries. *Nat. Protoc.* **2006**, *1*, 1987–1994. [[CrossRef](#)] [[PubMed](#)]

75. Friligou, I.; Papadimitriou, E.; Gatos, D.; Matsoukas, J.; Tselios, T. Microwave-assisted solid-phase peptide synthesis of the 60–110 domain of human pleiotrophin on 2-chlorotrityl resin. *Amino Acids* **2011**, *40*, 1431–1440. [[CrossRef](#)] [[PubMed](#)]
76. Eissler, S.; Kley, M.; Bächle, D.; Loidl, G.; Meier, T.; Samson, D. Substitution determination of Fmoc-substituted resins at different wavelengths: Substitution Determination of Fmoc-substituted Resins. *J. Pept. Sci.* **2017**, *23*, 757–762. [[CrossRef](#)]

Sample Availability: Not available.



© 2020 by the authors. Licensee MDPI, Basel, Switzerland. This article is an open access article distributed under the terms and conditions of the Creative Commons Attribution (CC BY) license (<http://creativecommons.org/licenses/by/4.0/>).